Predictive Reference Signal Generator for Hybrid Electric Vehicles

Daniel Ambühl and Lino Guzzella, *Senior Member, IEEE*

Abstract—A novel model-based and predictive energy supervisory controller for hybrid electric vehicles (HEVs) is presented. Its objective is to minimize the fuel consumption (FC) of HEVs using only the information on the current state of charge (SoC) of the battery and data available from a standard onboard navigation system. This objective is achieved using a predictive reference signal generator (pRSG) in combination with a nonpredictive reference tracking controller for the battery SoC. The pRSG computes the desired battery SoC trajectory as a function of vehicle position such that the recuperated energy is maximized despite the constraints on the battery SoC. To compute the SoC reference trajectory, only the topographic profile of the future road segments and the corresponding average traveling speeds must be known. Simulation results of the proposed predictive strategy show substantial improvements in fuel economy in hilly driving profiles, compared with nonpredictive strategies. A parallel HEV is analyzed in this paper. However, the proposed method is independent of the powertrain topology. Therefore, the method is applicable to all types of HEVs.

Index Terms—Convex optimization, hybrid electric vehicles (HEVs), navigation system, predictive energy management, reference signal generator, topographic maps.

I. INTRODUCTION

HYBRID electric vehicles (HEVs) are typically characterized by the presence of an internal combustion engine (ICE) and an electric propulsion system with an appropriate buffer. This combination of two or more power sources allows for substantial improvement of the fuel economy. On the other hand, there is a new degree of freedom, namely, the power distribution between the engine and the electric motor, that must judiciously be exploited to achieve the best possible fuel economy. In the literature, this task is referred to as the *supervisory control* problem. Heuristic solutions, which are often based on simple rules or maps, can achieve near-optimal fuel economy for a specific vehicle and under standard driving conditions. Unfortunately, heuristic approaches are difficult to transfer to other vehicles and driving conditions and require cumbersome tuning at the beginning. For these reasons, there is a clear tendency toward supervisory controllers that are based on systematic optimizations that use physical models of the

The authors are with the Department of Mechanical and Process Engineering, Swiss Federal Institute of Technology Zurich, 8092 Zurich, Switzerland (e-mail: daniel.ambuehl@alumni.ethz.ch; lguzzella@ethz.ch).

vehicle and only require a few parameters to be known at the outset [1].

The performance of any supervisory controller strongly depends on the information available [2]. A truly optimal fuel consumption (FC) can be achieved only if the entire driving cycle is perfectly known *a priori*. Deterministic dynamic programming (DP) [3] can be used to find such an optimal solution. The resulting strategy is not causal but defines a benchmark to which any causal strategy can be compared.

For the case where no information on future driving conditions is available, optimal fuel economy cannot be guaranteed. Such nonpredictive controllers are derived in [4] using a deterministic approach and in [5] and [6] using stochastic DP. The resulting controllers are position independent.

For the case where a route is repeatedly driven, some information can be collected on each repetition. This information is then used with stochastic DP to compute a position-dependent controller [7], [8].

In a case where some information on the trip is available from a navigation system, it can be exploited to improve the existing solutions. In [9], such an approach has been presented using DP. This paper focuses on such a case, wherein the only information available is the topographic profile and the average traveling speed on each of the road segments of the planned trip. The position of the vehicle is determined by a navigation system. The destination of the trip is specified by the driver at the outset. In case the driver does not specify the destination, it can be estimated from previously recorded driving cycles, as shown in [10]. Knowledge of the current position and the destination, combined with standard onboard navigation maps, allows the evaluation of the topographic profile and the average traveling speeds for each road segment of the trip. A predictive energy management is developed in this paper that exploits this information to minimize the FC.

The main idea of the supervisory control system presented in this paper is as follows: The starting point is a nonpredictive equivalent consumption-minimization strategy (ECMS) [4], [11]–[17]. This ECMS is extended by penalizing the deviation of the battery state of charge (SoC) from a reference value. If this reference value is kept constant, then such a strategy provides good fuel economy, as long as the battery is sufficiently large to absorb all the energy made available during recuperation events. If the amount of energy available for recuperation exceeds that limit, as, for instance, in hilly driving profiles, then the performance of the ECMS with a constant SoC reference value considerably decreases. This is a consequence of the fact that if the upper SoC limit is reached during braking or downhill driving phases, some energy cannot
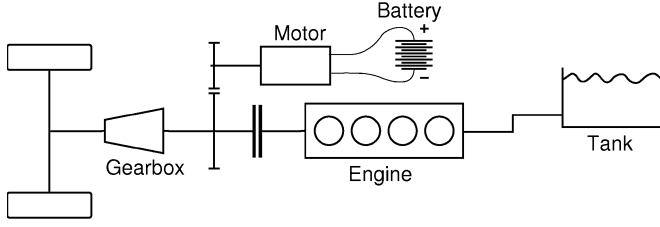
Fig. 1. Topology of a full parallel hybrid electric powertrain.

be recuperated but must be wasted in the conventional brakes. The predictive reference signal generator (pRSG) presented in this paper utilizes the available information on the future driving profile to compute a reference trajectory for the SoC that avoids this situation. This reference trajectory is computed from information about the actual position of the vehicle and the future elevation profile together with the planned average traveling speed during the trip. This information allows for an estimation of future recuperation phases. Simple energetic considerations allow the identification of the corresponding changes in the SoC during these recuperation phases. Once these SoC changes are identified, the SoC reference trajectory can efficiently be synthesized such that the lower and upper bounds of the batteries SoC are respected.

This paper is organized as follows: The model of the vehicle used in this paper is described in Section II. Section III briefly reviews the nonpredictive ECMS approach and shows its deficiencies in nonstandard driving conditions. The pRSG is introduced in Section IV. Finally, the benefits of applying the proposed pRSG are shown in Section V.

II. MODEL OF THE HYBRID POWERTRAIN

The vehicle analyzed in this paper is a full parallel HEV, i.e., the engine and the electric motor act on the same shaft, and there is a controllable clutch that can decouple the engine from the powertrain. This topology is illustrated in Fig. 1. The vehicle parameters subsequently used are those of a midsize passenger car with a mass of 1580 kg, a maximum power of the engine of 80 kW, a maximum power of the electric motor (EM) of 25 kW, and a battery (BT) with a capacity of 6.2 Ah at a nominal voltage of 230 V. The energy content of this battery is comparable with the traction battery used in the Generation III Toyota Prius.

As discussed in [18] and [19], a quasi-static "backward" approach is used to model the vehicle. This choice is motivated by the problem statement, as follows: The speed profile $v(t)$ is externally prescribed, i.e., it is considered to be a disturbance defined by the test cycle or the driver. The road grade γ is also modeled as a disturbance. For a given gear-switching strategy, the speed profile and the road grade determine the speed ω_{GB} and the torque T_{GB} at the gearbox (GB) input as

$$\omega_{GB} = f_{GB,\omega}(v, \gamma) \tag{1}$$
$$T_{GB} = f_{GB,T}(v, \gamma). \tag{2}$$

The torque T_{GB} at the GB input must be provided by the motor or by the engine satisfying the torque balance as

$$T_{GB} = T_{ICE} + T_{EM}. \tag{3}$$

The torques of the engine and the motor are limited, respectively, to

$$T_{ICE} \in [0, T_{ICE,max}(\omega)] \tag{4}$$
$$T_{EM} \in [T_{EM,min}(\omega), T_{EM,max}(\omega)]. \tag{5}$$

If the torque balance in (3) cannot be fulfilled during propulsion ($T_{GB} > 0$) due to the limits of the engine and the motor torque, this situation corresponds to an infeasible driving profile, and it is assumed that this case is not encountered. On the other hand, the situation where the torque balance is not fulfilled during deceleration ($T_{GB} < 0$) corresponds to (partially) conventional braking, and it can occur. In this situation, the engine is shut off, the electric motor is recuperating at $T_{EM,min}$, and the conventional brakes provide the remaining torque $T_{GB} + T_{EM,min}$ seen at the torque coupler.

As a consequence of the torque balance in (3), the operation points of the powertrain are fully determined by choosing either the engine torque or the torque of the motor. For consistency with the common literature, the motor torque is chosen as the control input. Normalized with the requested torque at the GB, the control signal u is defined as the torque split factor

$$u = \frac{T_{EM}}{T_{GB}}. \tag{6}$$

The torque at the engine results from (3) and (6) as

$$T_{ICE} = (1 - u) \cdot T_{GB}. \tag{7}$$

This equation reveals that pure electric driving is commanded by $u = 1$, and the engine is then shut off. The FC of the engine is given by a quasi-static map of the fuel mass flow $\overset{*}{m}_f$, depending on the engine torque T_{ICE} and speed ω_{ICE}, which is equal to the GB input speed ω_{GB} if the clutch is closed. The fuel mass flow results in

$$\overset{*}{m}_f = \begin{cases} f_{ICE}\left((1 - u) \cdot T_{GB}, \omega_{GB}\right), & \text{if } u < 1 \\ 0, & \text{if } u = 1. \end{cases} \tag{8}$$

On the electric side, the motor is also modeled with a quasi-static map of the electric power P_{EM} as a function of the torque T_{EM} and speed ω_{GB} as

$$P_{EM} = f_{EM}(T_{GB} \cdot u, \omega_{GB}). \tag{9}$$

This electric motor power P_{EM} is delivered from or to the battery that is modeled with an equivalent circuit model, as presented in [18]. The resulting battery current is given by

$$I_{BT} = \frac{V_{oc}(\xi) - \sqrt{V_{oc}(\xi)^2 - 4R_i(\xi)P_{EM}}}{2R_i(\xi)} \tag{10}$$

where $V_{oc}(\xi)$ and $R_i(\xi)$ are the open circuit voltage and the inner resistance of the battery at the actual SoC ξ, respectively.

The SoC of the battery is the only state variable of this model and results from current integration as

$$\frac{d\xi}{dt} = -\frac{I_{BT}}{Q_0} \tag{11}$$

with an initial condition $\xi(t = 0) = \xi_0$. The parameter Q_0 is the nominal battery capacity. The sign convention used here is in accordance with [14], where a positive current I_{BT} stands for discharging the battery. The SoC of the battery is physically limited to $[0, 1]$. To prevent the battery from excessive wear, the operation of the battery is only allowed in some limited range

$$\xi \in [\xi_{\min}, \xi_{\max}] \qquad (12)$$

which is given by hard constraints that lie within the physical SoC limits. These hard constraints are defined by the manufacturer of the battery pack. In this paper, the state constraints are set to $\xi_{\min} = 0.4$ and $\xi_{\max} = 0.7$, in accordance with [20].

Effects caused by changes of the temperatures of the battery, the electric motor, and the engine are neglected.

III. NONPREDICTIVE ENERGY MANAGEMENT

The goal of the supervisory controller is to find an optimal torque split factor $u^o(t)$ that minimizes the FC of the vehicle over a driving cycle. Furthermore, charge sustenance must be guaranteed; otherwise, the optimal control policy would simply deplete the battery over the driving cycle. For the case where full information on the driving cycle is available, charge sustenance is achieved by requesting the final SoC to be equal to the initial SoC, i.e., $\xi(t_f) = \xi(0)$. For the case where no or only limited information is available, this condition, in general, cannot be met. Penalizing the deviation of the SoC from a predefined reference value can be used to keep the SoC within the desired bounds. This is explained in more detail in the following section.

A. ECMS

This section presents a formulation of the ECMS that is slightly different from other formulations [4], [11]–[17]. In this section, it is assumed that no information on future driving conditions is available.

As previously mentioned, the cost function $J(u)$ is extended such that it penalizes not only the FC but, also, any SoC deviations from a not-yet-specified reference value $\xi_{\text{ref}}(t)$ as

$$J = \int_0^{t_f} \left\{ H_l \cdot \overset{*}{m}_f(u) + \alpha \left(\frac{\xi_{\text{ref}}(\tau) - \xi(\tau)}{\Delta\xi_{\text{nrm}}} \right)^{2q} \right\} d\tau. \qquad (13)$$

Here, t_f is the duration of the driving cycle, H_l is the lower heating value of the fuel, α is a weighting factor, and $q \in \mathbb{N}$ determines the order of the SoC penalty term. The SoC penalty function is normalized such that for all values of q, the penalty for the largest tolerable SoC deviation $\Delta\xi_{\text{nrm}}$ is equal to α.

As shown in Appendix A, the torque split factor is evaluated as the minimizer of the instantaneous equivalent FC, i.e.,

$$u = \arg \min_{\tilde{u}} \{ P_f(\tilde{u}) + s(\xi) \cdot P_{i,\text{BT}}(\xi, \tilde{u}) \}. \qquad (14)$$

Here, $P_f(u) = H_l \overset{*}{m}_f(u)$ is the consumed fuel power, and $P_{i,\text{BT}}(u) = V_{\text{oc}}(\xi) \cdot I_{\text{BT}}(\xi, u)$ is the inner battery power, where $V_{\text{oc}}(\xi)$ is the state-dependent open-circuit voltage of the battery.

TABLE I
PARAMETERS FOR THE ECMS

Parameter	Value	Unit
s_0	2.8	-
T_i	100	s
ξ_{ref}	0.55	-
$\Delta\xi_{nrm}$	0.1	-
q	2	-
T_h	500	s
α	2000	W

The equivalence factor $s(\xi)$ in (14) plays a crucial role in the ECMS; it trades off chemical against electric power. If the equivalence factor $s(\xi)$ is very large, then the ECMS tends to recharge the battery in almost all operating points. If the equivalence factor $s(\xi)$ is very small, then the ECMS favors pure electric driving. It is obvious that $s(\xi)$ is crucial for charge sustenance. In previous publications, various approaches of equivalence factors have been proposed [4], [11]–[17]. In this paper, the equivalence factor is chosen as

$$s(\xi(t)) = s_0 + \int_0^t \frac{\xi_{\text{ref}}(\tau) - \xi(\tau)}{T_i} d\tau \\ + \tilde{\alpha} \cdot \frac{(\xi_{\text{ref}}(t) - \xi(t))^{2q-1}}{Q_0 V_{\text{oc}}(\xi(t))}. \qquad (15)$$

This choice is motivated by optimal control theory [21]. Its derivation and the definition of the parameters s_0, T_i, and $\tilde{\alpha}$ are explained in Appendix A, and the values are given in Table I.

The strategy presented in this section can be applied without any information on the future driving conditions. For lack of a better choice, the reference SoC $\xi_{\text{ref}}(t)$ is usually chosen to be constant. Notice that in a real vehicle the battery SoC cannot directly be measured. Several approaches have been proposed to estimate this variable. In [22], an extended Kalman filter has been presented to estimate the SoC using measurements of the terminal current I_{BT} and voltage V_{BT} of the battery. The algorithm relies on a higher-order physical model of the battery.

It is important to note that the ECMS, as presented here, allows for reference tracking if $\tilde{\alpha} > 0$. This fact will be used in Section IV for the pRSG.

B. Results and Limitations of the ECMS

The nonpredictive charge-sustaining ECMS presented in Section III-A is now compared with the global optimum obtained using DP. However, no nonpredictive strategy can guarantee perfect charge sustenance. Therefore, the nonpredictive ECMS is simulated first with an initial SoC of $\xi(0) = 0.55$, achieving some final state $\xi(t_f)$. The DP solution is then evaluated using these initial and final conditions on ξ. Since the precision of the achieved final state is crucial to yielding a proper evaluation, numerical issues in the DP algorithm must be treated appropriately, as discussed in [23]. This procedure of evaluating the nonpredictive strategy against the global optimal strategy with identical initial and final states yields a "fair" comparison of the two strategies without the need for
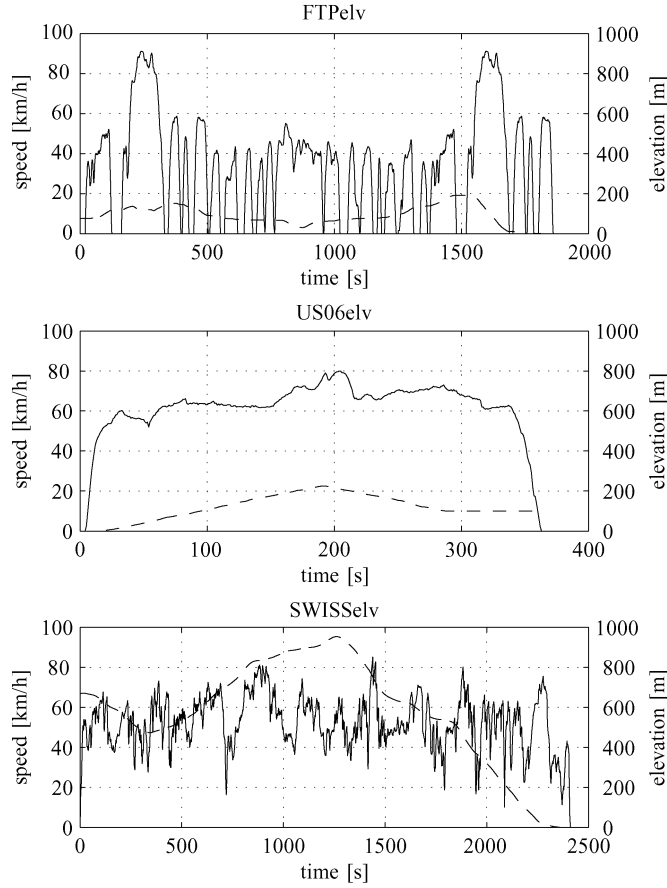
Fig. 2. Three driving cycles with (solid) speed and (dashed) topographic profiles.

TABLE II
SIMULATION RESULTS FOR THE ECMS

Cycle	FC (ECMS/DP) [l/100km]	rEC [%]
NEDC	5.46 / 5.33	+2.4
CADC	6.72 / 6.71	+0.2
ARB02	6.74 / 6.72	+0.3
FTP75	4.73 / 4.70	+0.7
FTPelv	4.55 / 4.20	+8.3
US06elv	8.07 / 7.64	+5.7
SWISSelv	3.90 / 3.54	+10.1

converting electric energy into fuel equivalent. The relative excess consumption defined as

$$rEC = \frac{\text{FC}_S - \text{FC}_{\text{DP}}}{\text{FC}_{\text{DP}}} \qquad (16)$$

is subsequently used to gauge the differences. Here, FC_S is the FC of any suboptimal strategy S, whereas FC_{DP} is the optimal FC evaluated by DP, with the initial and final conditions being those resulting from strategy S.

The driving cycles used for the evaluations are standard regulatory driving cycles, such as the NEDC, the CADC, the ARB02, and the FTP75. In addition, new driving cycles with topographic profiles are proposed in this paper. These cycles are labeled FTPelv, US06elv, and SWISSelv, whose profiles are shown in Fig. 2. The first cycle, i.e., FTPelv, is constructed by the addition of an altitude profile to the FTP75. The engine-off phase of the FTP75 of 600s has been removed for the FTPelv cycle because thermal effects are neglected. The altitude profile is obtained from the public database ADVISOR [24], namely, from its driving cycle "NREL2VAIL" that is a measured driving cycle. From this altitude profile, only the section from km 14 to km 32 is considered. The second cycle, i.e., US06elv, consists of a part of the speed profile of the regulatory driving cycle US06 and is scaled down to a maximum speed of 80 km/h. The altitude profile is extracted from topographic maps of a real representative road in the surroundings of

Zurich. The third cycle, i.e., SWISSelv, has been recorded in Switzerland and shows a relatively large amount of elevation changes.

The parameters used to evaluate the ECMS are summarized in Table I. They are tuned for the urban part of the Common Artemis Driving Cycle (CADC-Urban) and for the vehicle defined in Section II as follows: The parameter q is chosen as $q = 2$ to severely penalize large SoC deviations while having a soft penalty on small deviations. The reference SoC ξ_{ref} is centered between the lower and upper bounds, and the typical SoC deviation used for normalization is set to $\Delta\xi_{\text{nrm}} = 0.1$. The crucial parameters, however, are s_0, α, and T_i. In the first step, the basic equivalence factor s_0 is evaluated by using no SoC control, i.e., $\alpha = 0$ and $T_i = \infty$. An iterative search for the charge sustaining s_0 yields $s_0 = 2.77$ for CADC-Urban. Hence, a rounded value of $s_0 = 2.8$ is applied. The control parameters α and T_i are manually found such that the SoC deviation from the set point is less than 0.05.

The simulation results are summarized in Table II, which shows the FC and the relative excess consumption [see (16)]. These results show that the ECMS provides close to optimum FC for most flat standard cycles. The rEC only increases for driving cycles with long recuperation phases, such as the NEDC that has a long final deceleration phase. The situation changes substantially as soon as elevation changes are considered. This can be seen in the simulation results of the cycles FTPelv, US06elv, and SWISSelv, where the topographic profile leads to an rEC value ranging from 5.7% to 10.1%. This large difference between achieved FC and optimal FC is mainly due to the fact that the (nonpredictive) ECMS tries to keep the SoC near the reference value ξ_{ref} that is centered between the lower and upper constraints ξ_{min} and ξ_{max}, respectively. Consequently, if a longer recuperation phase occurs, only a fraction of the recuperable energy can be stored in the battery before its capacity limits are reached. Therefore, better approaches are necessary, which avoid this limitation, particularly in hilly driving profiles. As announced by [2], this can only be achieved by using predictive strategies.

IV. PREDICTIVE REFERENCE SIGNAL GENERATOR

This section introduces the proposed pRSG that generates a time-varying trajectory $\xi_{\text{ref}}(t)$. It exploits all available information of the future driving profile and respects the state constraints on the battery SoC. Fig. 3 schematically illustrates the extension of the existing ECMS with the pRSG.
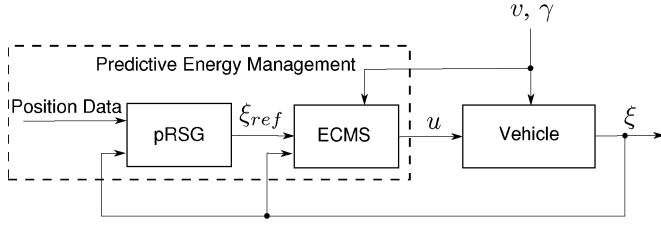
Fig. 3.   Block diagram of the pRSG-ECMS control system.

A. Method

The operation of an HEV can be categorized into two main types of operation. The first type of operation consists of all operations where the supervisory control can explicitly control the SoC by favoring or penalizing the use of the electric path. The time intervals during which the supervisory control is using this type of operation are referred to as *free* segments in this paper. The second type of operation consists of all operations where the supervisory control cannot explicitly control the SoC. This is typically the case when the powertrain is either in boosting mode ($T_{\mathrm{GB}} > T_{\mathrm{ICE,max}}$) or in recuperation mode ($T_{\mathrm{GB}} < 0$); the use of the electric path is purely determined by the driver/cycle. These time intervals are referred to as *fixed* segments. Since the SoC cannot explicitly be controlled during fixed segments, it can happen that the SoC violates its constraints, as discussed in the previous section. If this happens during a recuperation phase, some of the available recuperable energy must be wasted in the conventional brakes to respect the upper SoC constraint. Therefore, the ECMS needs to be extended to assure that information on the future driving profile is used to prevent such energy-wasting events. This objective is achieved by computing a time-varying reference trajectory for the SoC.

In a first step, the future fixed segments are identified from data of the navigation system. With this information, the future recuperable energies of the fixed segments are estimated and converted into future SoC changes. This is presented in Section IV-B.

In a second step, the SoC reference trajectory is synthesized on the basis of that information. The reference trajectory is assumed to be a piecewise affine function of time, where each affine segment corresponds to a free or fixed segment. The parameters of the affine SoC reference trajectory are computed such that the SoC constraints of the battery are not violated. The necessary computations can be formulated as a quadratic program (QP), which is solved very efficiently. The precise formulation of this optimization is presented in Section IV-C.

B. Prediction of Recuperation Time Segments

To predict the time segments where recuperation takes place, only the information provided by the navigation system is used, namely, the topographic profile [see (17)] and the average traveling speed on each road segment [see (18)] between the actual position and the destination, i.e.,

$$h_m = h(d_{h,m}) \tag{17}$$
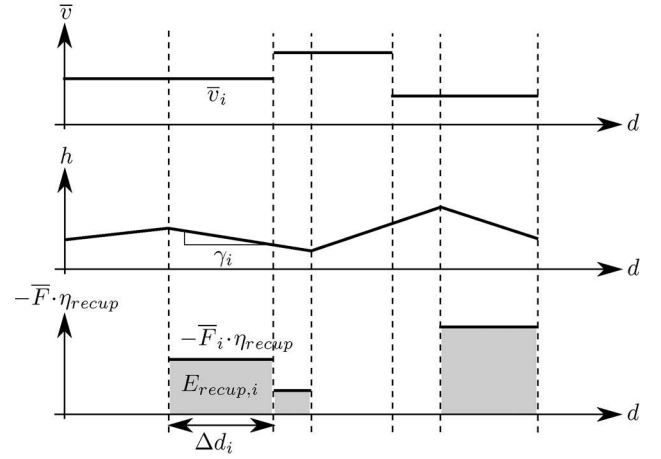$$\overline{v}_n = \overline{v}(d_{v,n}). \tag{18}$$

Fig. 4.   Data from the navigation system mapped to a common grid (top and center graphs) with the estimated recuperation force and the resulting recuperated energy due to elevation changes (bottom graph).

These data points are specified at discrete distances $d_{h,m}$ and $d_{v,n}$, respectively.

The two sets of data, which are represented in Fig. 4 (top and center graphs), are mapped to a common grid d_i as

$$d_i = d_{h,m} \cup d_{v,n} \tag{19}$$

as illustrated by the dashed vertical lines. As a result, each road segment with length Δd_i is characterized by its grade γ_i and its average speed $\overline{v}_i$.

The estimated force acting on the vehicle over the segment i is given by

$$\overline{F}_{\mathrm{unlim},i} = \frac{1}{2}\rho A_f c_d \overline{v}_i^2 + c_r m_v g \cos\gamma_i + m_v g \sin\gamma_i \tag{20}$$

where ρ is the air density, A_f is the frontal area of the vehicle, c_d is the aerodynamic drag coefficient, c_r is the rolling friction coefficient, m_v is the vehicle mass, and g is the gravitational acceleration.

During recuperation, high electric power flows can occur. These power flows can exceed the limitation $P_{\mathrm{el,min}}(< 0)$ of the electric path that includes the electric motor, the power converter, and the battery. Therefore, the (negative) force is limited by

$$\overline{F}_i = \max\left\{\overline{F}_{\mathrm{unlim},i}, \frac{P_{\mathrm{el,min}}}{\overline{v}_i \cdot \eta_{\mathrm{recup}}}\right\}. \tag{21}$$

The efficiency η_{recup} of the electric path during a recuperation phase is assumed to be constant. It accounts for all the losses from the wheels to the battery. The assumption of a constant η_{recup} could easily be relaxed by accounting for the operating-point-dependent efficiencies of all components. Such an expansion would, however, not change the main results of this paper.

Fig. 4 (bottom graph) illustrates the average force corrected with the recuperation efficiency for each road segment. The resulting estimated amount of potential energy that is recuperated
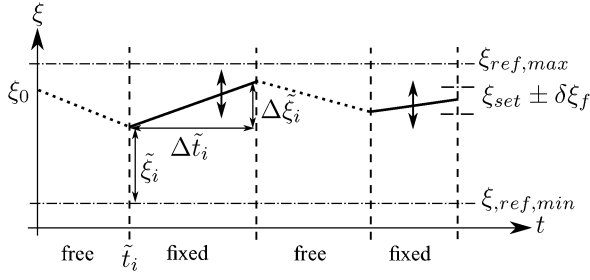
Fig. 5. Synthesis of the reference SoC trajectory by varying the initial condition $\tilde{\xi}_i$ for each recuperation phase.

over each interval i, indicated in the figure by the grey area, is given by

$$E_{\text{recup},i} = \begin{cases} -\overline{F}_i \cdot \Delta d_i \cdot \eta_{\text{recup}}, & \text{if } \overline{F}_i < 0 \\ 0, & \text{else.} \end{cases} \quad (22)$$

To derive the SoC reference trajectory, the recuperated energies $E_{\text{recup},i}$ are converted to the equivalent SoC changes $\Delta\tilde{\xi}_i$ using (23). The superscript˜is used in the following to denote variables of the fixed segments. For this conversion, the SoC is assumed to be near a given set point ξ_{set}. This assumption is made because the SoC level at which each recuperation will occur is unknown at this stage. The corresponding distances Δd_i are converted to time intervals using

$$\Delta\tilde{\xi}_i = \frac{E_{\text{recup},i}}{Q_0 V_{\text{oc}}(\xi_{\text{set}})} \quad (23)$$

$$\Delta\tilde{t}_i = \frac{\Delta d_i}{\overline{v}_i}. \quad (24)$$

To reduce the computational burden caused by generating the SoC reference trajectory, at each time step, all successive segments of recuperation are lumped into one segment of recuperation. Each of these N aggregated recuperation segments is then saved as a triple $\tilde{R}_i$ containing its (future) starting time, its duration, and the SoC change that is expected, e.g.,

$$\tilde{R}_i = \{\tilde{t}_i, \Delta\tilde{t}_i, \Delta\tilde{\xi}_i\}. \quad (25)$$

C. Synthesis of an SoC Reference Trajectory

The data about future expected recuperation segments $\tilde{R}_i$ are used to synthesize a reference trajectory for the SoC. As illustrated in Fig. 5, the problem that has to be solved is to find a piecewise-affine reference trajectory for the SoC that never violates the SoC boundaries. This trajectory consists of the fixed segments in which recuperation takes place and of the free segments that lie between two fixed segments. The fixed segments are known by their (future) starting time $\tilde{t}_i$, their duration $\Delta\tilde{t}_i$, and their change in SoC $\Delta\tilde{\xi}_i$. If the value of the SoC at each start of a fixed segment $\tilde{\xi}_i$ is defined, then the entire reference trajectory is determined. Hence, the SoC values $\tilde{\xi}_i$ are the unknowns that have to be found to be able to synthesize the SoC reference trajectory.

The reference trajectory ξ_{ref} must

- remain within the interval $\Omega = [\xi_{\text{ref,min}}, \xi_{\text{ref,max}}]$ at all times;
- keep the final SoC of the reference trajectory within a target interval $\Omega_f = [\xi_{\text{set}} - \delta\xi_f, \xi_{\text{set}} + \delta\xi_f]$;
- minimize the rate of change of the SoC during the free elements of the reference trajectory.

The last point is a choice that is made to extend the lifetime of the battery. In fact, minimizing the rate of change corresponds to minimizing the currents drawn from the battery, which is known to be beneficial for batteries [25].

1) Assumptions: The succeeding problem formulation is based on the following assumptions.

- The fixed segments only correspond to recuperation phases, i.e., $\Delta\tilde{\xi}_i > 0 \;\forall i = 1, \ldots, N$.
- The reference trajectory starts in a free segment.
- Fixed and free segments are alternating.
- The final segment is a fixed segment.

The assumption that the fixed segments only consist of recuperation phases is made because boosting phases, in general, are very short and are, therefore, considered to be disturbances. This assumption is not strictly necessary, but it considerably reduces the number of linear inequality constraints in the QP subsequently formulated. The assumption that the reference trajectory starts on a free segment is not restricting. If the vehicle is in a fixed segment when the optimization is started, then the reference signal up to the end of this segment is already fixed. Hence, the problem can be formulated to begin at the end of this first segment. The assumption that the fixed and free segments are alternating is a consequence of the aggregation of the recuperation phases, as discussed in Section IV-B. The last point simply reflects the assumption that the vehicle will be brought to standstill at the end of each trip.

2) Problem Formulation: The objectives previously mentioned can now be mathematically rephrased as follows:

- The SoC must be in the set Ω (lower bound, upper bound) and the final SoC (lower final state, upper final state) must be in the set Ω_f, i.e.,

$$\tilde{\xi}_i \geq \xi_{\text{ref,min}} - \varepsilon_i \quad (26)$$
$$\tilde{\xi}_i + \Delta\tilde{\xi}_i \leq \xi_{\text{ref,max}} + \varepsilon_i \quad (27)$$
$$\tilde{\xi}_N + \Delta\tilde{\xi}_N \geq \xi_{\text{set}} - \delta\xi_f - \varepsilon_f \quad (28)$$
$$\tilde{\xi}_N + \Delta\tilde{\xi}_N \leq \xi_{\text{set}} + \delta\xi_f + \varepsilon_f \quad (29)$$

where ε_i and ε_f are slackness variables introduced to guarantee the feasibility by softening the state constraints. Equation (26) has to be fulfilled for all $i = 1, \ldots, N$. The assumption that $\xi_{\text{set}} + \delta\xi_f < \xi_{\text{ref,max}}$ implies that (27) has to be fulfilled only for all $i = 1, \ldots, N - 1$. For $i = N$, (27) is always fulfilled when (29) is fulfilled. Summarizing, there are $2N + 1$ inequalities that must be satisfied.

- The minimization of the slopes of the free segments and the penalties on the slackness variables are expressed by

$$\min_x \left\{ \alpha_{\varepsilon,f} \cdot \varepsilon_f^2 + \sum_{i=1}^{N} \left(\frac{\Delta\hat{\xi}_i^2}{\Delta\hat{t}_i^2} + \alpha_\varepsilon \cdot \varepsilon_i^2 \right) \right\} \quad (30)$$
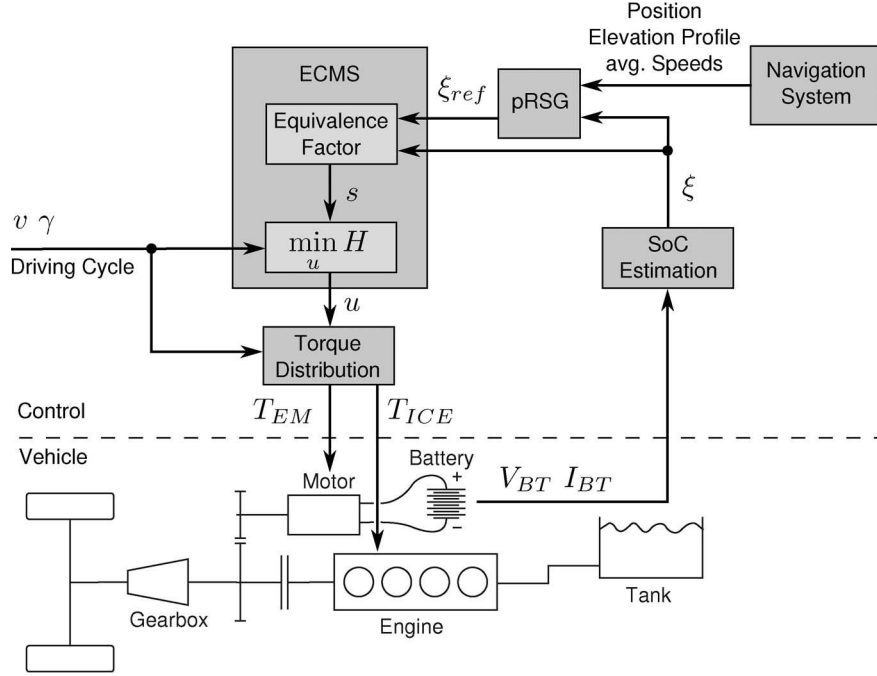
Fig. 6.   System-level block diagram of the pRSG-ECMS control system with the vehicle.

where

$$\Delta \hat{\xi}_i = \tilde{\xi}_i - (\tilde{\xi}_{i-1} + \Delta \tilde{\xi}_{i-1}) \tag{31}$$

$$\Delta \tilde{\xi}_0 = 0 \tag{32}$$

$$\Delta \hat{t}_i = \tilde{t}_i - (\tilde{t}_{i-1} + \Delta \tilde{t}_{i-1}) \tag{33}$$

$$\tilde{t}_0 = 0 \tag{34}$$

$$\Delta \tilde{t}_0 = 0. \tag{35}$$

The superscript $\hat{\ }$ denotes variables of the free segments. The unknown vector x of length $2N + 1$ is given by

$$x = [\tilde{\xi}_1, \dots, \tilde{\xi}_N, \varepsilon_1, \dots, \varepsilon_N, \varepsilon_f]^T \tag{36}$$

where $\tilde{\xi}_i$ represent the SoC at the beginning of each ith fixed segment. The slackness variables are penalized using the positive weights α_ε and $\alpha_{\varepsilon,f}$, respectively.

The problem defined in (26)–(36) can be formulated as a standard QP, i.e.,

$$\min_x x^T Q x + p^T x$$

$$\text{s.t.} \quad A x \le b. \tag{37}$$

The matrices Q, p, A, and b can be derived from (26)–(36) and are listed in Appendix B. The matrix Q is tridiagonal, and all the elements of the main diagonal are strictly positive. Furthermore, the other two diagonals each contain some zeros. With these properties, the matrix Q is positive definite. Consequently, the QP in (37) is convex and can be solved in polynomial time.

3) Synthesis of the Reference Trajectory: The desired SoC reference trajectory $\xi_j(t_j)$ is now determined by the first N

elements $\tilde{\xi}_i$ of the solution x of the QP, by the starting SoC value ξ_0, and by the SoC changes $\Delta \tilde{\xi}_i$, i.e.,

$$\xi_j = \begin{cases} \xi_0, & \text{if } j = 1 \\ \tilde{\xi}_i, & \text{if } j = 2i, \quad i = 1, \dots, N \\ \tilde{\xi}_i + \Delta \tilde{\xi}_i, & \text{if } j = 2i + 1, \quad i = 1, \dots, N \end{cases} \tag{38}$$

$$t_j = \begin{cases} 0, & \text{if } j = 1 \\ \tilde{t}_i, & \text{if } j = 2i, \quad i = 1, \dots, N \\ \tilde{t}_i + \Delta \tilde{t}_i, & \text{if } j = 2i + 1, \quad i = 1, \dots, N. \end{cases} \tag{39}$$

Since the SoC reference trajectory is calculated from data on the aggregated time grid [see (25)], it is projected back to the original time grid by linear interpolation and finally remapped from time to the positions d_i using (19).

D. ECMS with pRSG

At this point, the nonpredictive ECMS can be combined with the pRSG, as illustrated in Fig. 3. Instead of a constant value, the ECMS now obtains a time- or position-dependent reference value $\xi_{\text{ref}}(t)$. This reference signal requests that the SoC of the battery is lowered by the ECMS before some important recuperation phases occur. This ensures that most of the available energy can be recuperated. In the following, this predictive energy-management strategy is referred to as pRSG-ECMS. The block diagram in Fig. 6 shows the system consisting of the predictive controller and the vehicle on a system level.

V. RESULTS

A. Definition of Test Framework

Since both strategies, namely, the pRSG-ECMS and the standard ECMS, are causal, neither of them can guarantee that exactly the specified final SoC is achieved. Consequently, the
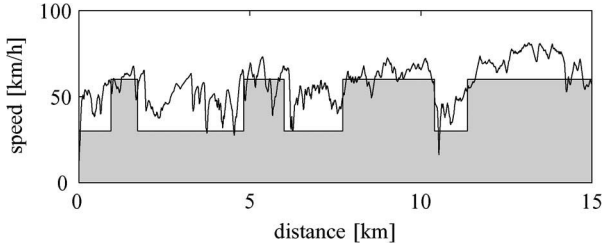
Fig. 7. Approximated data of the simulated average traveling speed (filled) as provided by the navigation system (first part of the SWISSelv cycle), together with the real driving cycle (solid line).

TABLE III
PARAMETERS FOR THE pRSG-ECMS

Parameter	Value	Unit
η_{recup}	0.7	-
ξ_{min}	0.4	-
ξ_{max}	0.7	-
$\delta\xi_f$	0.01	-
α_ε	10^8	s^{-2}
$\alpha_{\varepsilon,f}$	10^7	s^{-2}

resulting FC of each strategy over a driving cycle cannot be compared with the other because the change of the electric energy content in the battery over the cycle is not equal in both cases. Therefore, each strategy is compared with the corresponding global optimal solution. This optimal solution is evaluated for the same initial and final states as resulting from each strategy. The relative excess consumption rEC introduced in Section III-B is used in all cases to compare the results.

B. Simulation of the Navigation System

To assess the quality of the proposed method, simulations of all three cases (ECMS, pRSG-ECMS, and DP) must be carried out. The pRSG-ECMS requires the data provided by the navigation system to be available. These data points are derived from the exact driving profiles for simulation as follows.

1) The topographic data points provided by the navigation system are assumed to be exact. Therefore, the data points defined in the driving profile are used for the simulation and the prediction.

2) In contrast, the speed profile cannot exactly be predicted by the navigation system. Therefore, using the exact driving profile, an average speed is computed, which is used as the simulated output available from the navigation system. This approximation is very rough on purpose. Fig. 7 shows this approximation for the first part of SWISSelv. The algorithm that was used to construct the simulated average traveling speed is listed in Appendix C.

C. Simulation Results

This section shows the results of the simulations carried out for the three test cycles with elevation changes (FTPelv, US06elv, and SWISSelv). The parameters for the ECMS and the pRSG-ECMS are identical to assure that both strategies yield the same results on flat terrain. The parameters are listed in Table I. The additional parameters used for the pRSG are shown in Table III.

TABLE IV
SIMULATION RESULTS FOR THREE CYCLES WITH ELEVATION CHANGES

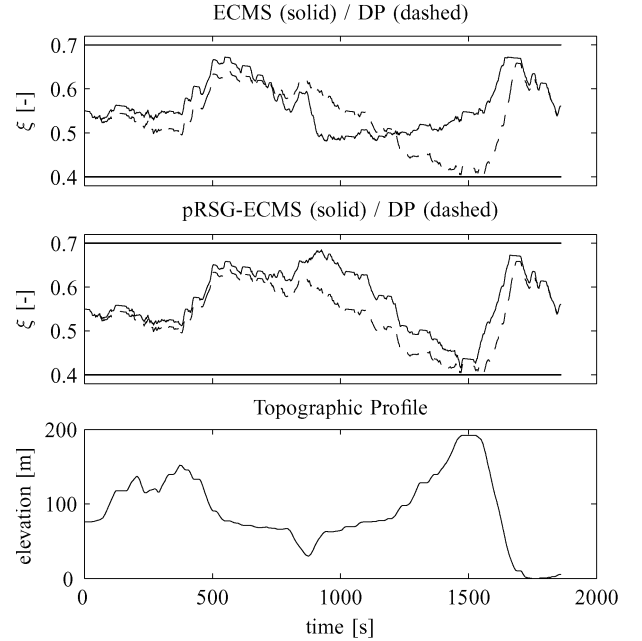| Cycle	Strategy	FC (Strategy/DP) [l/100km]	rEC [%]
FTPelv	ECMS	4.55 / 4.20	+8.3
	pRSG-ECMS	4.42 / 4.20	+5.2
US06elv	ECMS	8.07 / 7.64	+5.7
	pRSG-ECMS	7.45 / 7.45	+0.0(2)
SWISSelv	ECMS	3.90 / 3.54	+10.1
	pRSG-ECMS	3.63 / 3.54	+2.4

Fig. 8. SoC trajectories of ECMS versus DP and pRSG-ECMS versus DP for cycle FTPelv and its elevation profile.

The FC and the relative excess consumption of the two causal strategies are summarized in Table IV. In a hilly environment, the pRSG-ECMS performs considerably better than the ECMS. The FC with the pRSG-ECMS deviates by less than 5.1% from the optimal solution for the cycles investigated here. For the cycle US06elv, the pRSG-ECMS yields almost optimal FC. This is explained by the fact that the driving cycle has an almost constant speed near the value of 60 km/h, which closely matches the estimation of the navigation system. Furthermore, the altitude profile of this driving cycle shows a relatively uniform road grade, i.e., first ascending and then descending.

Figs. 8–10 show the state trajectories of the ECMS and the pRSG-ECMS with the corresponding optimal state trajectories obtained with DP (dashed). In addition, the topographic profile is shown to point out the interconnection between (future) elevation and SoC. These figures illustrate that, particularly for the US06elv, the state trajectory obtained with the pRSG-ECMS is closer to the optimal solution than that obtained with the standard ECMS. A comparison of the topographic profile with the SoC trajectory shows that the proposed strategy lowers the SoC before important recuperation events take place.
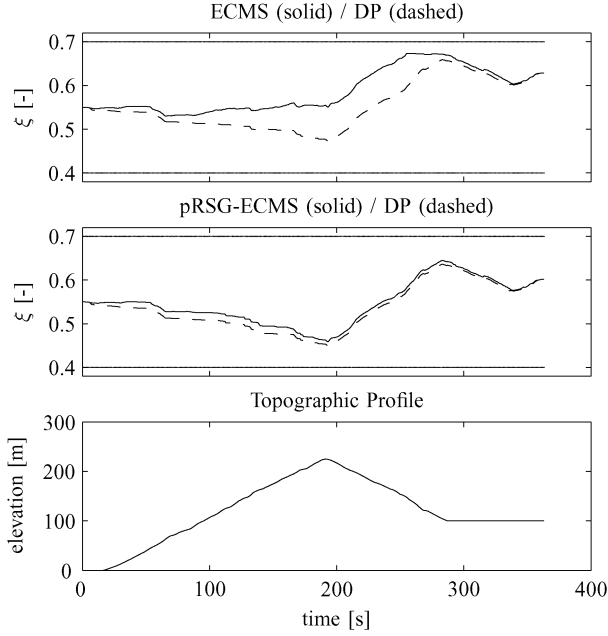
Fig. 9. SoC trajectories of ECMS versus DP and pRSG-ECMS versus DP for cycle US06elv and its elevation profile.
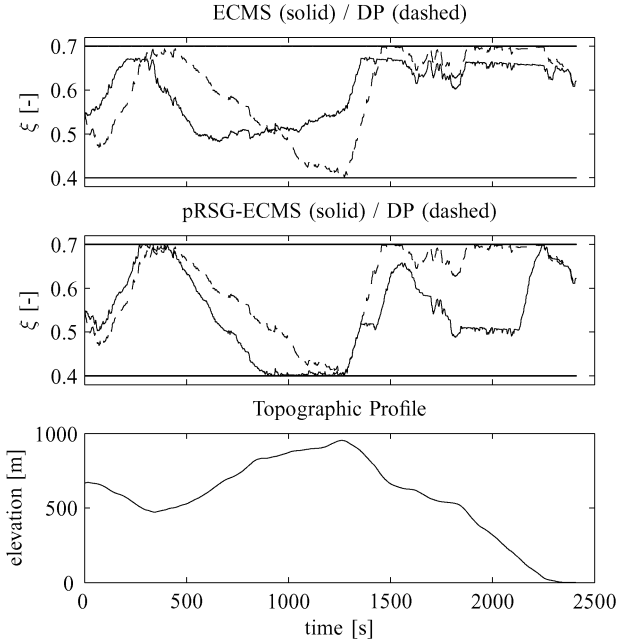

Fig. 10. SoC trajectories of ECMS versus DP and pRSG-ECMS versus DP for cycle SWISSelv and its elevation profile.

VI. Conclusion

A predictive energy-management strategy that yields considerably better fuel economy than standard ECMS when driving on hilly roads has been developed. The new approach only requires data available from standard navigation systems, such as the topographic profile and the average traveling speed for each road segment. The proposed strategy acts on two levels: The first level is a nonpredictive ECMS controller that is extended to be able to track a reference SoC. The second level is the predictive SoC reference signal generator, which uses the data provided by the navigation system. This reference trajectory

is chosen such that the amount of recuperated energy is maximized while respecting the SoC constraints of the battery. The proposed reference signal generator is applicable to all HEV topologies and all strategies that are able to track a reference SoC. Simulation results for a full parallel HEV shown in this paper illustrate the potential of the proposed new approach. Experiments for the validation of these results are currently being set up in collaboration with the industrial partner.

Appendix A
Derivation of the ECMS

From optimal control theory [21], it follows that the optimal control $u^o(t)$ must minimize the Hamiltonian [see (40)] at every time instant, as shown in (41). The Hamiltonian consists of the integrand of the cost functional [see (13)], the right-hand side of the state dynamics [see (11)], and a Lagrange multiplier $\lambda(t)$, i.e.,

$$H(\xi, u, \lambda) = H_l \cdot \overset{*}{m}_f(u) + \alpha \left(\frac{\xi_{\text{ref}} - \xi}{\Delta \xi_{\text{nrm}}} \right)^{2q}$$
$$- \lambda(t) \cdot \frac{I_{\text{BT}}(\xi, u)}{Q_0} \tag{40}$$

$$u^o = \arg\min_u H(\xi^o, u, \lambda^o). \tag{41}$$

The optimal Lagrange multiplier λ^o is given by

$$\lambda^o(\xi, t) = \frac{\partial \mathcal{J}^o(\xi, t)}{\partial \xi} \tag{42}$$

where $\mathcal{J}^o(\xi, t)$ is the optimal cost-to-go function.

Since, at this point, it is assumed that there is no knowledge available about future driving conditions, it is not possible to evaluate the optimal cost-to-go function $\mathcal{J}^o(\xi, t)$. Therefore, a (suboptimal) cost-to-go function is estimated as a function of the SoC but independent of time. The (suboptimal and time-invariant) cost-to-go function is estimated as follows: The cost functional in (13) penalizes FC and any SoC deviation from the reference value. The FC is assumed to consist of two parts. The first part represents the fuel energy $\mathcal{J}_{f,1}(\xi)$ that would be used to recharge or discharge the battery from the actual SoC back to the reference value. The second part represents the remaining fuel energy use $\mathcal{J}_{f,2}$, which is assumed to be independent of the current SoC. Therefore, the estimated cost-to-go function is written as

$$\mathcal{J}(\xi) = \mathcal{J}_{f,1}(\xi) + \mathcal{J}_{f,2} + \mathcal{J}_{\text{SoC}}(\xi) \tag{43}$$

where $\mathcal{J}_{\text{SoC}}$ denotes the cost due to SoC deviations from the reference value.

Since only the gradient of the cost-to-go function in the SoC is of interest [see (42)], the term $J_{f,2}$ does not need to be resolved. The fuel energy used to compensate the current SoC is approximated by

$$\mathcal{J}_{f,1}(\xi) \cong \frac{Q_0}{\eta_c} \int\limits_{\xi(t)}^{\xi_{\text{ref}}} V_{\text{oc}}(\tilde{\xi}) d\tilde{\xi}. \tag{44}$$

Here, $V_{oc}(\xi)$ is the open-circuit voltage of the battery, and η_c is the average conversion efficiency between chemical and electric energies. This conversion efficiency is assumed to be constant.

The SoC penalty term $\mathcal{J}_{SoC}$ is estimated based on the assumption that the SoC is brought back from the current value $\xi(t)$ to the reference value ξ_{ref} in time T_h. This assumed future SoC trajectory $\xi_{fut}(\tau)$ is assumed to be affine in time as

$$\xi_{fut}(\tau) = \xi(t) - \frac{\xi(t) - \xi_{ref}}{T_h} \cdot \tau. \tag{45}$$

The cost resulting from the second term of (13) combined with the assumed future SoC trajectory from (45) is

$$J_{SoC}(\xi) = \int_0^{T_h} \alpha \left(\frac{\xi_{ref} - \xi_{fut}(\tau)}{\Delta\xi_{nrm}} \right)^{2q} d\tau$$

$$= \frac{\alpha T_h}{1 + 2q} \cdot \left(\frac{\xi_{ref} - \xi(t)}{\Delta\xi_{nrm}} \right)^{2q}. \tag{46}$$

Hence, the estimation of the cost-to-go function obtained from (43), (44), and (46) is

$$\mathcal{J}(\xi) = \mathcal{J}_{f,1}(\xi) + \mathcal{J}_{f,2} + \mathcal{J}_{SoC}(\xi)$$

$$= \frac{Q_0}{\eta_c} \int_{\xi(t)}^{\xi_{ref}} V_{oc}(\tilde{\xi}) d\tilde{\xi} + J_{f,2} + \frac{\alpha T_h}{1 + 2q} \cdot \left(\frac{\xi_{ref} - \xi(t)}{\Delta\xi_{nrm}} \right)^{2q}. \tag{47}$$

The corresponding suboptimal and time-invariant Lagrangian multiplier resulting from (42) and (47) thus becomes

$$\lambda(\xi) = \frac{\partial \mathcal{J}(\xi)}{\partial \xi}$$

$$= -\frac{Q_0 V_{oc}(\xi)}{\eta_c} - \tilde{\alpha} \cdot (\xi_{ref} - \xi(t))^{2q-1} \tag{48}$$

with the substitution

$$\tilde{\alpha} := \frac{2q\alpha T_h}{(1 + 2q)\Delta\xi_{nrm}^{2q}}. \tag{49}$$

Summarizing, the suboptimal but causal control $u(\xi)$ is determined with (41), (40), and (48). These equations can be rewritten by substitution of the Lagrangian multiplier by a normalized quantity, i.e., the "equivalence factor"

$$s(\xi) = -\frac{\lambda(\xi)}{Q_0 V_{oc}(\xi)}. \tag{50}$$

Furthermore, the second term of the Hamiltonian [see (40)] that does not explicitly depend on u is omitted in the minimization of H with respect to u, since it does not affect the minimizer u. Therefore, the control signal follows from

$$u = \arg\min_{\tilde{u}} \left\{ H_l \overset{*}{m}_f(\tilde{u}) + s(\xi) \cdot V_{oc}(\xi) I_{BT}(\xi, \tilde{u}) \right\}$$

$$= \arg\min_{\tilde{u}} \left\{ P_f(\tilde{u}) + s(\xi) \cdot P_{i,BT}(\xi, \tilde{u}) \right\} \tag{51}$$

$$s(\xi) = \frac{1}{\eta_c} + \frac{\tilde{\alpha}}{Q_0 V_{oc}(\xi)} \cdot (\xi_{ref} - \xi(t))^{2q-1} \tag{52}$$

where $P_f(u) = H_l \overset{*}{m}_f(u)$ is the fuel power consumed by the engine, and $P_{i,BT}(\xi, u) = V_{oc}(\xi) I_{BT}(\xi, u)$ is the inner battery power for the actual torque split.

The average conversion efficiency η_c slightly varies with the driving profile. Therefore, its value is updated using a simple integrator with integration time T_i. Furthermore, $1/\eta_c$ is substituted by s_0 for convenience. The equivalence factor from (52) is finally given as

$$s(\xi(t)) = s_0 + \int_0^t \frac{\xi_{ref} - \xi(\tau)}{T_i} d\tau + \frac{\tilde{\alpha}(\xi_{ref} - \xi(t))^{2q-1}}{Q_0 V_{oc}(\xi)}. \tag{53}$$

APPENDIX B
MATRICES OF THE QP

$$Q_{i,j} = \begin{cases} \frac{1}{\Delta\hat{t}_i^2} + \frac{1}{\Delta\hat{t}_{i+1}^2}, & \text{if } i = j = 1, \ldots, N-1 \\ \frac{1}{\Delta\hat{t}_N^2}, & \text{if } i = j = N \\ \alpha_\varepsilon, & \text{if } i = j = N+1, \ldots, 2N \\ \alpha_{\varepsilon,f}, & \text{if } i = j = 2N+1 \\ -\frac{1}{\Delta\hat{t}_i^2}, & \text{if } i = j - 1 = 2, \ldots, N \\ -\frac{1}{\Delta\hat{t}_i^2}, & \text{if } i = j + 1 = 1, \ldots, N-1 \\ 0, & \text{else} \end{cases} \tag{54}$$

$$p_i = \begin{cases} -\frac{2\xi_0}{\Delta\hat{t}_N^2}, & \text{if } i = N \wedge N = 1 \\ -\frac{2\xi_0}{\Delta\hat{t}_1^2} + \frac{2\tilde{\xi}_1}{\Delta\hat{t}_1^2}, & \text{if } i = 1 \wedge N > 1 \\ -\frac{2\tilde{\xi}_{i-1}}{\Delta\hat{t}_i^2} + \frac{2\tilde{\xi}_{i-1}}{\Delta\hat{t}_{i+1}^2}, & \text{if } i = 2, \ldots, N-1 \wedge N > 2 \\ -\frac{2\tilde{\xi}_{N-1}}{\Delta\hat{t}_N^2}, & \text{if } i = N \wedge N > 1 \\ 0, & \text{if } i = N+1, \ldots, 2N+1 \end{cases} \tag{55}$$

$$A_{i,j} = \begin{cases} -1, & \text{if } i = 1, \ldots, 2N-1 \wedge j = i \\ -1, & \text{if } i = 1, \ldots, N \wedge j = i + N \\ 1, & \text{if } i = N+1, \ldots, 2N-1 \wedge j = i - N \\ -1, & \text{if } i = 2N \wedge j = N \\ -1, & \text{if } i = 2N \wedge j = 2N+1 \\ 1, & \text{if } i = 2N+1 \wedge j = N \\ -1, & \text{if } i = 2N+1 \wedge j = 2N+1 \\ 0, & \text{else} \end{cases} \tag{56}$$

$$b_i = \begin{cases} -\xi_{ref,min}, & \text{if } i = 1, \ldots, N \\ \xi_{ref,max} - \Delta\tilde{\xi}_{i-N}, & \text{if } i = N+1, \ldots, 2N-1 \\ -\xi_{set} + \delta\xi_f + \Delta\tilde{\xi}_N, & \text{if } i = 2N \\ \xi_{set} + \delta\xi_f - \Delta\tilde{\xi}_N, & \text{if } i = 2N+1. \end{cases} \tag{57}$$

APPENDIX C
CONSTRUCTION OF THE SIMULATED DATA
OUTPUT OF THE NAVIGATION SYSTEM

It is assumed that the navigation system only distinguishes between urban, extraurban, and highway with the corresponding regulatory speed limits of 50, 80, and 120 km/h, respectively. (Obviously, any other choice would work as well.) The average traveling speeds assigned to each of these zones are assumed to be 30, 60, and 100 km/h, respectively.

To obtain the simulated estimated navigation data $\overline{v}(d)$ from the exact speed profile $v(t)$ of the test cycle, the following steps are carried out:

1) converting the speed signal into an index signal $i(t)$ using threshold values of 55 and 85 km/h. The indexes $i = 1, 2, 3$ stand for urban, extraurban, or highway;
2) filtering the index signal with a noncausal zero-phase low-pass filter with time constant $\tau = 30$ s;
3) rounding the filtered index signal back to integers;
4) replacing the indexes back to traveling speeds of 30, 60, or 100 km/h;
5) mapping of the average speed signal $\overline{v}(t)$ from time to position $\overline{v}(d)$.

REFERENCES

[1] A. Sciarretta and L. Guzzella, "Control of hybrid electric vehicles," *IEEE Control Syst. Mag.*, vol. 27, no. 2, pp. 60–70, Apr. 2007.
[2] M. Salman, M.-F. Chang, and J.-S. Chen, "Predictive energy management strategies for hybrid vehicles," in *Proc. IEEE Conf. Veh. Power Propuls.*, Chicago, IL, Sep. 7–9, 2005, pp. 21–25.
[3] R. E. Bellman, *Dynamic Programming*. Princeton, NJ: Princeton Univ. Press, 1957.
[4] D. Ambühl, A. Sciarretta, C. Onder, L. Guzzella, S. Sterzing, K. Mann, D. Kraft, and M. Küsell, "A causal operation strategy for hybrid electric vehicles based on optimal control theory," in *Proc. 4th Symp. Hybrid Veh. Energy Manage.*, Braunschweig, Germany, Feb. 14–15, 2007, pp. 318–331.
[5] E. D. Tate, J. W. Grizzle, and H. Peng, "Shortest path stochastic control for hybrid electric vehicles," *Int. J. Robust Nonlinear Control*, vol. 18, no. 14, pp. 1409–1429, 2008.
[6] D. F. Opila, D. Aswani, R. McGee, J. A. Cook, and J. Grizzle, "Incorporating drivability metrics into optimal energy management strategies for hybrid vehicles," in *Proc. IEEE Conf. Decision Control*, Cancun, Mexico, Dec. 2008, pp. 4382–4389.
[7] L. Johannesson, M. Åsbogård, and B. Egardt, "Assessing the potential of predictive control for hybrid vehicle powertrains using stochastic dynamic programming," *IEEE Trans. Intell. Transp. Syst.*, vol. 8, no. 1, pp. 71–83, Mar. 2007.
[8] L. Johannesson and B. Egardt, "A novel algorithm for predictive control of parallel hybrid powertrains based on dynamic programming," in *Proc. 5th IFAC Symp. Adv. Autom. Control*, Monterey, CA, Aug. 20–22, 2007.
[9] T. van Keulen, B. de Jager, A. Serrarens, and M. Steinbuch, "Optimal energy management in hybrid electric trucks using route information," in *Proc. Les Rencontres Scientifiques de l'IFP, Adv. Hybrid Powertrains*, Rueil-Malmaison, France, Nov. 25–26, 2008.
[10] J. Froehlich and J. Krumm, "Route prediction from trip observations," presented at the SAE World Congr. Exhibition, Detroit, MI, 2008.
[11] A. Brahma, Y. Guezennec, and G. Rizzoni, "Optimal energy management in series hybrid electric vehicles," in *Proc. Amer. Control Conf.*, Chicago, IL, 2000, pp. 60–64.
[12] G. Paganelli, G. Ercole, A. Brahma, Y. Guezennec, and G. Rizzoni, "General supervisory control policy for the energy optimization of charge-sustaining hybrid electric vehicles," *JSAE Rev.*, vol. 22, no. 4, pp. 511–518, Oct. 2001.
[13] S. Delprat, T. Guerra, and J. Rimaux, "Optimal control of a parallel powertrain: From global optimization to real time control strategy," in *Proc. IEEE 55th Veh. Technol. Conf.*, Birmingham, AL, May 6–9, 2002, vol. 4, pp. 2082–2088.
[14] A. Sciarretta, M. Back, and L. Guzzella, "Optimal control of parallel hybrid electric vehicles," *IEEE Trans. Control Syst. Technol.*, vol. 12, no. 3, pp. 352–363, May 2004.
[15] P. Pisu and G. Rizzoni, "A comparative study of supervisory control strategies for hybrid electric vehicles," *IEEE Trans. Control Syst. Technol.*, vol. 15, no. 3, pp. 506–518, May 2007.
[16] R. Beck, A. Bollig, and D. Abel, "Comparison of two real-time predictive strategies for the optimal energy management of a hybrid electric vehicle," in *Proc. Les Rencontres Scientifiques de l'IFP, New Trends Engine Control, Simul. Model.*, Rueil-Malmaison, France, Oct. 2–4, 2006, pp. 239–246.
[17] J. T. Kessels, M. W. Koot, P. P. van den Bosch, and D. B. Kok, "Online energy management for hybrid electric vehicles," *IEEE Trans. Veh. Technol.*, vol. 57, no. 6, pp. 3428–3440, Nov. 2008.
[18] L. Guzzella and A. Amstutz, "CAE tools for quasi-static modeling and optimization of hybrid powertrains," *IEEE Trans. Veh. Technol.*, vol. 48, no. 6, pp. 1762–1769, Nov. 1999.
[19] L. Guzzella and A. Sciarretta, *Vehicle Propulsion Systems: Introduction to Modeling and Optimization*, 2nd ed. Berlin, Germany: Springer-Verlag, 2007.
[20] O. Sundström, L. Guzzella, and P. Soltic, "Optimal hybridization in two parallel hybrid electric vehicles using dynamic programming," in *Proc. 17th IFAC World Congr.*, Seoul, Korea, Jul. 6–11, 2008, pp. 4642–4647.
[21] M. Athans and P. L. Falb, *Optimal Control*. New York: McGraw-Hill, 1966.
[22] O. Barbarisi, F. Vasca, and L. Glielmo, "State of charge Kalman filter estimator for automotive batteries," *Control Eng. Pract.*, vol. 14, no. 3, pp. 267–275, Mar. 2006.
[23] O. Sundström, D. Ambühl, and L. Guzzella, "On implementation of dynamic programming for optimal control problems with final state constraints," *Oil Gas Sci. Technol.—Rev. IFP*, 2009 (Reprint: Proc. of Les Rencontres Scientifiques de l'IFP, Adv. in Hybrid Powertrains, Rueil-Malmaison, France, 2008). [Online]. Available: http://ogst.ifp.fr/index.php?option=forthcoming&Itemid=18&lang=en
[24] K. Wipke, M. Cuddy, and S. Burch, "ADVISOR 2.1: A user-friendly advanced powertrain simulation using a combined backward/forward approach," *IEEE Trans. Veh. Technol.*, vol. 48, no. 6, pp. 1751–1761, Nov. 1999.
[25] L. Serrao, Z. Chehab, Y. Guezennec, and G. Rizzoni, "An aging model of Ni-MH batteries for hybrid electric vehicles," in *Proc. IEEE Conf. Veh. Power Propuls.*, Chicago, IL, Sep. 7–9, 2005, pp. 78–85.

Daniel Ambühl was born in Davos, Switzerland, in 1979. He received the Master's degree in mechanical engineering from the Swiss Federal Institute of Technology (ETH) Zurich, Zurich, Switzerland, in 2005, where he is currently a doctoral student with the Measurement and Control Laboratory, ETH Zurich.

His research interests include modeling, optimization, and control of dynamic systems with application to automotive systems.

Lino Guzzella (SM'05) was born in Zurich, Switzerland, in 1957. He received the Diploma in mechanical engineering and the Dr.Sc.Techn. degree in control engineering from the Swiss Federal Institute of Technology (ETH) Zurich, in 1981 and 1986, respectively.

From 1987 to 1989, he was with the R&D Department, Sulzer Bros., Winterthur, Switzerland. From 1989 to 1991, he was an Assistant Professor of automatic control with the Electrical Engineering Department, ETH Zurich. He then joined Hilti R&D, Schaan, Principality of Lichtenstein, where he was the Head of the Mechatronics Department from 1992 to 1993. He is currently a Professor of thermotronics with the Department of Mechanical and Process Engineering, ETH. His research interests are modeling of dynamic systems and nonlinear and robust control and the application of these ideas to thermal and, particularly, automotive systems.